Retinal Temperature Determination Based on Photopic Porcine Electroretinogram

Ossi Kaikkonen, Teemu T. Turunen, Anna Meller, Johanna Åhlgren, and Ari Koskelainen

Abstract*—*Objective: **Subthreshold retinal laser therapy (SLT) is a treatment modality where the temperature of the retinal pigment epithelium (RPE) is briefly elevated to trigger the therapeutic benefits of sublethal heat shock. However, the temperature elevation induced by a laser exposure varies between patients due to individual differences in RPE pigmentation and choroidal perfusion. This study describes an electroretinography (ERG)-based method for controlling the temperature elevation during SLT.** ***Methods:*** **The temperature dependence of the photopic ERG response kinetics were investigated both ex vivo with isolated pig retinas and in vivo with anesthetized pigs by altering the temperature of the subject and recording ERG in different temperatures. A model was created for ERG-based temperature estimation and the feasibility of the model for controlling SLT was assessed through computational simulations.** ***Results:*** **The kinetics of the photopic in vivo flash ERG signaling accelerated between 3.6 and 4.7%/°C, depending on the strength of the stimulus. The temperature dependence was 5.0%/°C in the entire investigated range of 33 to 44°C in ex vivo ERG. The simulations showed that the method is suitable for determining the steady-state temperature elevation in SLT treatments with a sufficiently long laser exposure and large spot size, e.g., during $>$ 30 s laser exposures with $>$ 3 mm stimulus spot diameter.** ***Conclusions:*** **The described ERG-based temperature estimation model could be used to control SLT treatments such as transpupillary thermotherapy.** ***Significance:*** **The introduced ERG-based method for controlling SLT could improve the repeatability, safety, and efficacy of the treatment of various retinal disorders.**

***Index Terms*—Electrophysiology, electroretinography, porcine retina, retinal laser therapy, temperature.**

I. Introduction

SUBTHRESHOLD laser therapy (SLT) is a treatment modality where laser irradiation of the fundus induces a transient heat shock in the retinal pigment epithelium (RPE) and surrounding tissues. SLT aims to trigger the therapeutic effects of heat shock without causing cell death in retinal tissues. The exact mechanism for the treatment effect is uncertain, but the cellular effects of subthreshold heat shock include the increased production of heat shock proteins [1]–[3], modulation of the oxidant/antioxidant balance [4], decrement of Bruch's membrane thickness [5], and reduction of angiogenesis [6]. SLTs have shown therapeutic benefit in the treatment of diabetic macular edema [7]–[10], proliferative diabetic retinopathy [11], [12], macular edema due to branch retinal vein occlusion [9], [10], central serous chorioretinopathy (CSC) [10], [13]–[18], and age-related macular degeneration (AMD) [19]–[21].

The therapeutic window for SLT is narrow. Although there is uncertainty about the key mechanisms responsible for delivering the therapeutic effect, the ratio between laser power causing increased HSP70 production and the laser power causing cell death in the irradiated site has been most extensively studied. Laser powers between 50 and 80% of the power causing cellular damage have been reported to trigger increased HSP70 production in the RPE and choroid [22]–[24].

A key challenge in delivering SLT has been the lack of thermal dosimetry. Variability in physiological characteristics such as RPE pigmentation and choroidal vascularization between patients and different retinal areas leads to significant variability in the temperature elevation caused by a standard laser exposure. Therefore, treatments delivered without thermal dosimetry produce differing thermal doses between patients and require a wide safety margin below the thermal dose causing tissue damage. As the therapeutic window is narrow, an excessive safety margin may lead to subtherapeutic and inconsistent treatments. Determining the local relation between laser power and temperature elevation in the fundus would allow individualized treatment power adjustment for the reliable delivery of the wanted thermal dose. This would reduce the required safety margin between the targeted thermal dose and the thermal dose causing tissue damage, potentially improving treatment efficacy and safety, and ensuring more consistent treatment outcomes.

Corneal electroretinography (ERG) is a non-invasive technique for registering electrical signals from retinal neurons in response to light stimulation with ocular and skin electrodes. The kinetics of the ERG signal is temperature-dependent and presents a potential probe for temperature monitoring of the retina and the closely connected RPE layer during laser-induced hyperthermia. The temperature dependence of dark-adapted

Manuscript received April 14, 2021; revised August 16, 2021; accepted August 29, 2021. Date of publication September 10, 2021; date of current version January 20, 2022. This project was supported by Business Finland, project number: 1786/31/2018. *(Ossi Kaikkonen and Teemu T. Turunen contributed equally to this work.) (Correspondence author: Ari Koskelainen.)*

Ossi Kaikkonen and Teemu T. Turunen are with the Department of Neuroscience and Biomedical Engineering, Aalto University School of Science, Finland.

Anna Meller and Johanna Åhlgren are with the Laboratory Animal Centre, Helsinki Institute of Life Science (HiLIFE), University of Helsinki, Finland.

Ari Koskelainen is with the Department of Neuroscience and Biomedical Engineering, Aalto University School of Science, Espoo 12200 FI-00076, Finland (e-mail: ari.koskelainen@aalto.fi).

Digital Object Identifier 10.1109/TBME.2021.3111533

ERG responses generated by rod cells has been quantified in mice, both *ex vivo* and *in vivo* [25], [26], providing a proof-of-concept for ERG-based retinal temperature determination. However, several constraints arise for temperature determination from laser application and clinical feasibility when used during retinal laser therapy. The spatial and temporal resolution are central constraints of the method, as the temperature should be determined in a time window shorter than the laser exposure from low amplitude local ERG signals that arise from the treated area.

Local ERG signals can be recorded with focal ERG techniques (fERG) where only a small retinal area is stimulated with flickering light. Both rod and cone-driven fERG can be recorded non-invasively from human subjects [27]. However, rod photoreceptor cells have slow light response kinetics, and their signaling saturates at daylight. Cone photoreceptor cells have faster light responses than rods, and unlike rods, they do not saturate even in bright background lights. Due to the differences between rod and cone systems, rod-driven focal ERG (fERG) techniques require elaborate controls to mitigate artefacts induced by scattered stimulus light [28] and require longer recording times for denoising the signal. Therefore, utilizing the cone system enables ERG-based temperature determination from smaller retinal areas with higher temporal resolution than rod-driven focal ERG.

In this study, we investigated the temperature dependencies of cone-driven ERG signaling kinetics in photopic conditions by analyzing ERG flash responses recorded at different temperatures, both *ex vivo* with isolated retinas from pigs and *in vivo* with anesthetized domestic pigs. The dimensions of the pig eye and the ERG signals registered from the porcine retina are similar to those of a human eye, which makes pigs suitable model animals for humans. The kinetics of the a- and b-wave complex of photopic *in vivo* ERG signals was found to accelerate by 3.6 to 4.7%/°C depending on the stimulus strength. To test the feasibility of the cone-driven ERG signal for temperature determination during laser treatments, we simulated the effect of realistic signal noise and response amplitudes to temperature determination precision. The ERG signal amplitude is proportional to the stimulated retinal area, allowing the conversion of the signal amplitudes to stimulus spot sizes needed for eliciting the focal ERG signal. Our simulations show that the technique can estimate porcine retinal temperature with < 0.5°C precision from a 3 mm retinal spot with 14 second temporal resolution, suggesting that the method is applicable as thermal dosimetry for clinical procedures such as transpupillary thermotherapy.

II. Methods

The use and handling of the animals were in accordance with the Finnish Act on the Protection of Animals Used for Scientific and Educational Purposes (497/2013) and the Government Decree on the Protection of Animals Used for Scientific and Educational Purposes (564/2013) and approved by the Project Authorization Board in Finland (project license ESAVI-30526-2019, approved Nov 1st 2019).

A. Ex Vivo Experiments

Pig eyes were collected either from a nearby animal facility or from a slaughterhouse immediately after the slaughter of the animals. Eyes were cleaned from excess tissue and opened on-site along the equator of the eye with scalpel and scissors while submerged in bicarbonated Ames solution (Merck group / Sigma-Aldrich, Darmstadt, Germany) at room temperature. The vitreous was removed from the posterior eyecups and the open eyecups were transferred to the laboratory in a light-tight container in Ames' solution continuously bubbled with carbogen gas (5% CO2 and 95% O2) to maintain stable pH and to provide oxygen supply for the tissue.

At the laboratory, 3 mm punches were taken from the eyecup using a disposable biopsy needle (Integra LifeSciences Corporation, New Jersey, USA), and the retina was isolated from the punch. The isolated piece of the retina was inserted photoreceptors upwards on a filter paper glued to a sample holder. The sample holder composed of two fitting polycarbonate parts, and the retina was gently squeezed between the two parts so that sides of the retina were mechanically supported, but the center of the retina laid freely on the filter paper [25]. The sample holder was placed on a light-tight Faraday's cage to minimize the electrical disturbances to recordings. The retina was perfused from both sides with a continuous flow (flow rate 4 ml/min) of bicarbonated Ames' medium preheated to 38°C and bubbled with carbogen gas. The pH of the solution was 7.5. All laboratory procedures were conducted under dim red light to avoid excessive light.

1) ERG Recording and Light Stimulation: The transretinal ERG signal was recorded using two Ag/AgCl pellet electrodes (EP2, World Precision Instruments, Florida, USA) connected to distal and proximal sides of the retina through the perfusion channels of the sample holder. The recorded signal was low-pass filtered with a cut-off frequency of 1 kHz and sampled at 10 kHz. The data was analyzed with Matlab 2018a (Mathworks, Natick, United States).

The output of a 530 nm fiber-coupled LED (M530F2 + M28L02, Thorlabs, New Jersey, USA) was projected onto the retina for stimulation and background illumination. Beam homogeneity was confirmed with a beam camera (SP503U, Ophir-Spiricon Inc, Utah, USA), and the irradiance of the beam was calibrated using an optical power meter (PM121D, Thorlabs). ERG responses were elicited with 1 ms flashes of light with 10 Hz repetition frequency against a constant background of 21 lx to ensure the suppression of rod signaling.

2) Experimental Procedure: The sample holder allowed retinal temperature alterations to be performed in under 30 seconds. The temperature of the retina was monitored with small thermistors (TT5-10KC3-72, diameter 0.5 mm, Tewa Termico Ltd., Leczna, Poland) placed inside the solution channels on both sides of the retina so that the distance between the retina and the thermistor was less than 2 mm. The nutrition solution flowing on both sides of the retina was warmed with resistive wire heaters coiled around the inlet perfusion tubings close to the retina. The heating power was controlled with a custom-made proportional-integral-derivative (PID) controller. The temperature on the nutrition solution perfusing the proximal side of the

retina was continuously kept at 37°C and the temperature of the nutrition solution perfusing the distal (photoreceptor) side was altered in order to cycle retinal temperature [25].

The temperature of the retina was first stabilized to 37°C, which was used as the reference temperature throughout the experiments. The retina was stimulated with 1 ms pulses repeated at 10 Hz frequency, varying the stimulus strength to find the flash stimulus strength that produces the fastest cone-driven b-wave. The temperature of the outer retina was then cycled between the reference temperature of 37°C and temperatures between 33 and 44°C, while continuously stimulating it with the stimulus strength producing the fastest cone-driven b-wave. The flash strength was fine-tuned during the experiment if the sensitivity of the retinal sample changed significantly.

B. In Vivo Experiments

5 male domestic pigs (Sus scrofa domestica) were acquired from a local farmer. At least 14 days of acclimatization time was provided for each animal before experiments. Animals were at the age of 14 – 16 weeks (15.3 ± 0.7, mean ± std) and weighted 41 – 51 kg (47 ± 3.7, mean ± std) at the time of the experiment day. No signs of sickness or any other symptoms were evident at the time of induction of anesthesia.

Animals were housed at the Large animal facility of the Laboratory Animal Centre of the University of Helsinki. Toys, straw, and fresh hay were available as enrichments. The solid floor of the pen was covered with wood shavings (Pölkky, Pölkky Oy, Kuusamo, Finland). Food (Pekoni 1 mure or Kombi Nasu, Suomen rehu, Hankkija Oy, Hyvinkää, Finland) was provided twice a day, and fresh tap water was available ad libitum. Room temperature was 19 ± 1°C and relative humidity 45 – 60%. The pen was cleaned once per day. In addition to natural light from windows, lights were on from 7 am to 15 pm.

1) Terminal Anesthesia Protocol: The pigs were premedicated with injectable midazolam 0.2 mg/kg given to oral or nasal mucosa. After 15 minutes, the animals were sedated with a mixture of medetomidine 0.08 mg/kg and midazolam 0.5 mg/kg subcutaneously (SC). After sedation (approximately 10 min), ketamine was given 5 mg/kg SC. Preoxygenation of the pigs prior to intubation was done by a mask with 100% of oxygen. Intravenous (IV)-cannulation was done to the auricular vein. The cannula with fixation wings was taped with skin tape to the ear. Meloxicam was given 5 mg/kg SC for multimodal analgesia. Ringer infusion was given at a rate of 8 ml/kg/h. For the induction of the anesthesia, propofol was given IV (at maximum 3 mg/kg). After induction, the pigs were intubated with cuffed endotracheal tube (Rüsch, Rüschelit Super Safety Clear) and connected to a ventilator (Dräger Primus SW 4.5n, Dräger Medical GmbH, Lübeck, Germany) and the pigs were mechanically ventilated by a volume control mode using tidal volumes of 7 – 9 ml/kg for the duration of the anesthesia. The anesthesia was maintained by total intravenous anesthesia (TIVA), using constant rate infusions (CRI) of propofol (2 – 4.4 mg/kg/h), fentanyl (0.003 – 0.005 mg/kg/h) and midazolam (0.4 – 0.7 mg/kg/h). First fentanyl was given as a bolus of 0.0055 mg/kg IV. The anesthesia level and the vital parameters (heart rate, respiratory rate, saturation, end tidal CO2) were monitored constantly and the infusion rates were adjusted to meet the individual needs of each animal.

Duration of the anesthesia (from intubation to euthanasia) variated between 3 hours 45 minutes to 5 hours. The pigs were placed on a prone position on the table. The eyes of the anesthetized pig were moistened with Viscotears 2 mg/g eye gel (Dr. Gerhard Mann chem.-pharm. Fabrik GmbH, Berlin, Germany) repeatedly during the experiments. The eye that was not currently stimulated was closed with tape. The pupils were dilated with tropicamide (Oftan Tropicamide 5 mg/ml, Santen Oy, Tampere, Finland) and the corneas anesthetized with oxybuprocaine hydrochloride (Oftan Obucain 4 mg/ml, Santen Oy, Tampere, Finland). The body temperature was continuously monitored with a nasopharyngeal temperature probe inserted ca. 10 cm deep into the nasal cavity (DMQ-DAG-20-N0, Cables and Sensors, Orlando, USA). The nostrils were blocked to minimize the fluctuation of nasopharyngeal temperature due to gas exchange. At the end of the procedure, the pigs were euthanized by 100 mg/kg pentobarbital IV.

These pigs have had similar anesthesia protocol on the previous day as part of different study. All pigs had recovered normally from the previous anesthesia.

2) ERG Recording and Light Stimulation: EEG cup electrodes (Reusable EEG cup electrode Silver/Silver Chloride, Technomed, Maastricht, The Netherlands) were used as the reference and ground electrodes for the ERG recordings. The locations for electrode placement were shaved, cleaned, and scrubbed with abrasive gel (Nuprep, Weaver and Company, Colorado, USA) to improve skin conductivity. The reference electrode was attached on the skin at the outer corner of the eye and the ground electrode at the ear with conductive paste (Ten20, Weaver and Company) and tape. A Dawson, Trick and Lizkow (DTL) thread electrode (Unimed Electrode Supplies Ltd, Surrey, United Kingdom) was placed on the cornea above the rim of the lower eyelid to serve as an ERG recording electrode.

A custom-made full-field globe stimulator was used for light stimulation. A white LED (CMA1840-0000-000N0U0A40G, Cree Inc., Durham, North Carolina, USA) was used to illuminate the diffuse inner surface of the stimulator to produce a constant background and flash stimulation. The corneal illuminance was measured using a light meter (LM-100, Amprobe, Everett, Washington, USA) placed at the opening of the globe, and the measured illuminance value was converted to luminance. Steady illumination of 300 cd·m-2 was used as a light-adapting background throughout the in vivo experiment. 1 ms flashes with 8 Hz frequency were used to elicit the photopic ERG responses. Signals were amplified and bandpass filtered (1 to 1000 Hz) by a biosignal amplifier system (FE232 Dual Bio Amp and PowerLab 8/35, 8 Channel Recorded, ADInstruments Ltd., Sydney, Australia), and acquired using a data acquisition system (cDAQ-9179 and NI9215, National instruments, Texas, USA).

3) Experimental Procedure: The body temperature was allowed to stabilize to a steady value between 36.6 and 39.3°C depending on the natural body temperature of the pig. The studied eye was stimulated with 4.8 $cd \cdot s \cdot m^{-2}$ flashes with 8 Hz frequency in a steady 300 $cd \cdot m^{-2}$ background until the

kinetics of the flash responses had stabilized, implying a steady light adaptation state. A set of ERG flash responses, i.e., a response family, was registered with increasing flash strengths between 0.3 and 19 cd·s·m^{-2} with $\sqrt[4]{2}$ relative increments, 8 Hz stimulation frequency, and 4 seconds of stimulation per flash strength. The latter 2 seconds of responses acquired with each flash strength were averaged for further analysis. The same procedure was repeated to collect the response family from the other eye.

The body temperature of the pig was then decreased or increased 1.8 to 2.5°C from the stable body temperature, leading to final temperatures ranging from 36.6 to 39.4°C. The lowering of body temperature was conducted with wet towels placed on the pig and cool packs placed below the pig near the femoral and brachial arteries. Additionally, constant room temperature air current was directed on the pig with Bair Hugger™ patient warming system (3M, Minnesota, United States). The body temperature was increased with the Bair Hugger™ patient warming system by placing an air mattress (Bair Hugger™ Pediatric Full Body Blanket, 31000), with a constant flow of 42°C air through it, on the pig. Additionally, a blanket was placed on the air mattress. After reaching a steady temperature, response families were registered from both eyes with the same procedure as in normal body temperature.

C. Temperature Estimation From ERG Responses

As the temperature of the retina increases, the kinetics of the ERG signal accelerates. This can be modeled as time axis scaling, shown in Eq. 1, where response f_1 is transformed into f_1' by scaling its time axis by a factor β, with the moment of the impulse stimulus set to t = 0. Time axis scaling can be used to approximate the effects of a mild temperature change ΔT on the waveform of the signal according to Eq. 2, where α is the temperature dependence of ERG kinetics acceleration. Henceforth, the transformation shown in Eq. 1 is termed the time scaling transformation.

$$f_1'\ (t)\ = f_1\ \left(\frac{t}{\beta}\right) \tag{1}$$

$$\beta = e^{\alpha \Delta T} \tag{2}$$

The difference in signaling kinetics between signals $f_1(t)$ and $f_2(t)$ can be quantified into a single parameter β_{opt}, henceforth termed the optimal time scaling parameter, by finding the time axis scaling that maximizes a similarity measure between $f_2(t)$ and $f_1'(t)$. A method for computing β_{opt} is shown in Eq. 3, where Pearson's correlation is used as the similarity measure. The computation of the time-scaling feature involves the use of one hyperparameter, t_{max}, which determines the time interval for calculating the correlation between the responses. In this study, t_{max} was chosen to be 50 ms for *ex vivo* responses and 25 ms for in vivo responses to include the a- and b-wave complex. The feature value was computed using a parameter sweep at the interval of $\beta \in [0.6,\ 1.4]$.

$$\beta_{opt} = \underset{\beta}{argmax}\left(corr\left(f_1\left(\frac{t}{\beta}\right), f_2\left(t\right)\right)\right), \in \left[0, t_{max}\left(1 - \frac{1-\beta}{2}\right)\right] \tag{3}$$

The optimal time scaling parameter can then be related to the difference in temperature ΔT between the two responses through its temperature dependence α. With small temperature changes near normal body temperature, $ln(\beta_{opt})$ is expected to depend linearly on temperature, as shown in Eq. 2. Eq. 4 shows how β_{opt} is used to determine changes in retinal temperature.

$$\Delta T\ = T_1\ -\ T_2 = \frac{\ln\left(\beta_{opt}\right)}{\alpha} = \frac{1}{\alpha}\ ln\left(\underset{\beta}{argmax}\left(corr\left(f_1\left(\frac{t}{\beta}\right), f_2\left(t\right)\right)\right)\right), \in \left[0, t_{max}\left(1 - \frac{1-\beta}{2}\right)\right] \tag{4}$$

The *ex vivo* temperature cycles involved recording ERG responses at the reference temperature of 37°C before and after acquiring ERG responses at a stable altered temperature. The time scaling feature was computed between the ERG response recorded at the altered temperature and both the reference ERG responses acquired at 37°C before and after the temperature alteration. The value used in the final analysis was a weighted average between the two, where the weight was based on the time proximity of the reference ERG response acquisitions to the acquisition of the ERG response at the altered temperature. The time scaling feature was computed for each *in vivo* temperature alteration by comparing responses recorded at the two different steady temperatures, elicited with the same flash strength.

D. Simulations

The feasibility of ERG based temperature determination during SLT was analyzed through simulations. In SLT, a small spot on the fundus is heated with laser, and a focal ERG signal is recorded within the heated area. The focal ERG response amplitude is proportional to the extent of the stimulated retinal area, and the signal-to-noise ratio (SNR) of the ERG signal decreases when the size of the stimulation spot is decreased.

The a- and b-waves, respectively, of the focal and full-field ERG have very similar waveforms [29]–[31] unless focal ERG is recorded from an area with significantly altered signaling [32]. As the full-field ERG responses were acquired from healthy pigs without known retinal abnormalities, the waveforms of the a- and b-waves found in full-field ERG responses are expected to be similar to the waveforms of focal ERG responses. The simulations utilize the full-field ERG responses as waveform templates to represent the waveforms of focal ERG.The simulations were conducted by combining realistic noise from ERG recordings and amplitude scaled versions of full-field ERG responses. The full-field ERG responses were recorded from anesthetized pigs with 8 Hz stimulation frequency. The traces of ERG noise were isolated from separate recordings. As laser treatments are

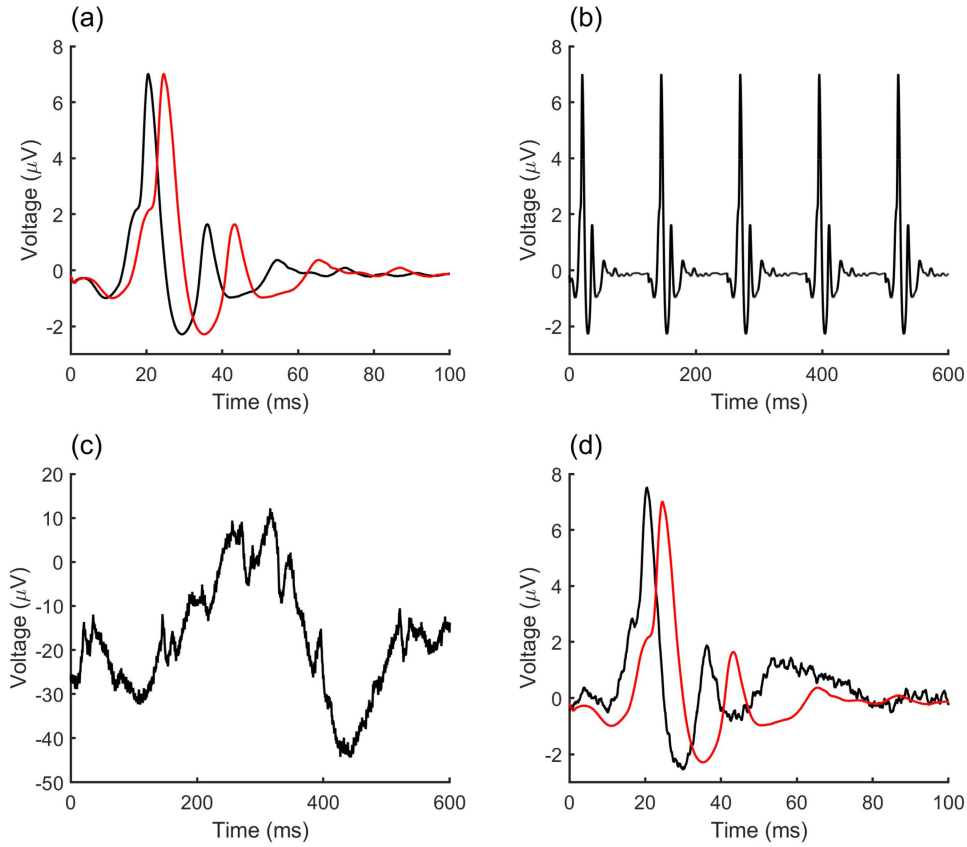

Fig. 1. (a) A full-field ERG response (black) with an amplitude scaled to 8 μV and the same response with a scaled time axis (red). (b) The black response of panel a replicated into a series of responses. Panel b shows only five consecutive responses although the number of responses in the series can vary freely in the simulations. (c) ERG noise superimposed on the response series of panel b. (d) Averaged response calculated from a noisy response series containing 40 responses (black) together with the noise-free time axis scaled response from panel a (red). The difference between feature value calculations of the responses in panel a and panel d determines the error caused by noise.

typically delivered using a fundus lens contacting the cornea, such a lens (HR Wide Field, Volk Optical Inc., Ohio, USA) was placed on the cornea supported by a lens mount (Steady Mount, Volk Optical Inc.) to simulate a realistic laser treatment configuration. A DTL electrode was placed on the eye under the fundus lens to enable signal acquisition.

The simulation algorithm, illustrated in Fig. 1, comprises repeating the following steps with different randomizations at each iteration and with different signal amplitudes and numbers of averaged responses.

1) Select a full-field ERG response at random.
2) Downscale the amplitude of the full-field ERG response to mimic a focal ERG response.
3) Generate another version of the scaled full-field ERG response applying a time axis scaling transformation (see Eq. 1) using a random number between 0.8 and 1.1 as the time scaling parameter β. (Fig. 1a)
4) Create a series, where the response resulting from step 3 is repeated n times. (Fig. 1b)
5) Select a noise series at random and select a random interval of the series corresponding to the length of the response series of step 4.
6) Overlay the response series from step 4 over the noise trace from step 5. (Fig. 1c)
7) Compute an averaged response from the noisy response series from step 6.
8) Compute the optimal time scaling parameter between the noise-free response from step 1 and the noisy response from step 7 using Eq. 3. (Fig. 1d)
9) Compute the optimal time scaling parameter between the noise-free responses from step 1 and step 3 (Eq. 3).
10) Calculate the error caused by noise as the difference between the optimal time scaling parameter from step 8, computed with signal noise, and the optimal time scaling parameter from step 9, computed without signal noise.

The simulation process was iterated with different noise recordings, full-field ERG responses, numbers of averaged responses, and signal amplitudes. The root-mean-square (RMS) error for temperature determination caused by noise in one of the compared signals is computed according to Eq. 5 with each combination of signal amplitude and number of averaged responses. In Eq. 5 K denotes the total number of simulation iterations performed with a given response amplitude and number

of averaged responses.

$$E_1 = \sqrt{\frac{1}{K}\sum_{k=1}^{K}\left(\beta_{opt,\,noisy,\,k} - \beta_{opt,\,noise-free,\,k}\right)^2} \quad (5)$$

Eq. 6 shows a closed-form notation to estimate the total RMS error in the time axis scaling feature caused by signal noise in both of the compared signals. a_1 and a_2 are amplitudes of the compared ERG signals calculated from the peak of the a-wave to the peak of the b-wave, n_1 and n_2 are the numbers of averaged signals to generate the responses for comparison, and c is a constant, which depends on the noise levels of the ERG recording configuration and stimulation frequency. As the error contributions from both of the signals are independent, the total error is given by the Euclidean norm. The constant c was fitted to data where noise was added to only one of the compared ERG signals, while the other was kept noise-free.

$$E_{RMS} = \sqrt{{E_1}^2 + {E_2}^2} = c\sqrt{\frac{1}{{a_1}^2 n_1} + \frac{1}{{a_2}^2 n_2}} \quad (6)$$

III. Results

A. Temperature-Dependence of Pig ERG Signal in a Broad Temperature Range

The temperature dependence of the a- and b-wave complex of photopic flash ERG signals was investigated by comparing the signaling kinetics of responses recorded at different temperatures from stamps isolated from pig retinas. The experiments with isolated retinas enabled the recording of photopic ERG responses in a broad temperature range by changing the temperature of the nutrition solution superfusing the retina. The temperature of the outer retina was varied between a reference temperature of 37°C and temperatures ranging from 33 to 44°C while continuously stimulating the retina with a 10 Hz flash flicker and recording *ex vivo* ERG. The light sensitivity of each retinal stamp was characterized by eliciting ERG responses with a series of increasing flash strengths, i.e., by collecting a response family in the reference temperature of 37°C before cycling the temperature of the retina. With dim stimuli, the time-to-peak of the b-wave reduces with increasing stimulus strengths, eventually reaching its lowest value, followed by a deceleration when the flash strength is increased further (see Fig. 2a). The flash strength producing the fastest cone-driven b-wave was selected from an *ex vivo* ERG response family and used during the temperature cycling. This protocol enabled the stimulation of two retinas with different sensitivities with flash strengths eliciting similar ERG waveforms. After a temperature alteration, flash responses recorded in a stable temperature were averaged, and the averaged responses were compared to responses recorded at the reference temperature to assess the amount of signaling kinetics acceleration/deceleration caused by the temperature change. A constant background light of 21 lx was used throughout the temperature cycles to suppress a potential rod cell contribution to the ERG signals.

Fig. 2b shows the perfusate temperature (black trace) and the temperature determined from recorded ERG signals (red trace) during two temperature alterations. The time intervals of stable ERG responses recorded in reference and altered temperature are illustrated with black and red marks, respectively. Figs. 2c and 2d present the two sets of flash responses recorded before and during the temperature alterations of Fig. 2b. The extent of change in the ERG response kinetics was quantified by determining an optimal time scaling parameter between the ERG response recorded at the altered temperature and ERG responses recorded at 37°C before and after the temperature alteration (see Methods for details). The dashed trace in Figs. 2c and 2d show the ERG response recorded at the reference temperature scaled with the optimal time scaling parameter, which maximizes the correlation between the transformed ERG response and the response recorded in the altered temperature.

A total of 44 temperature cycles were performed with 8 stamps from 6 retinas. Fig. 3 shows the logarithm of the optimal time scaling parameter plotted against the temperature change from the reference for each temperature alteration. The logarithm of the optimal time scaling parameter value changed by 5.0%/°C in the used lighting conditions, and the change was highly linear on this semi-log scale at the investigated temperature interval of 33 – 44°C, similarly as found before for the kinetics of scotopic b-wave [25], [26].

B. Effect of Stimulus Strength on ERG Signal Temperature-Dependence in Anesthetized Pigs

To investigate the temperature dependence of ERG flash response kinetics in conditions corresponding to a clinical situation, e.g., to those prevailing during a laser treatment, we recorded full-field ERG at different temperatures from anesthetized pigs. The stimuli were presented over a bright background illumination, which is required in a clinical laser treatment procedure to mitigate the light adaptation caused by the laser beam, and to enable fundus imaging in the visible spectrum. The *in vivo* experiments involved changing the body temperature of anesthetized pigs and recording full-field ERG flash responses with a broad range of flash strengths. The body temperature was allowed to stabilize to the natural body temperature before recording the first response family, followed by a temperature alteration, stabilization and recording another response family. Responses elicited with the same flash strength at different temperatures were compared to assess the temperature dependent acceleration or deceleration of response kinetics. A total of 6 temperature steps were performed with 5 pigs and response families were recorded from both eyes. An identical number of temperature alterations involved raising and lowering the body temperature to mitigate the confounding effects of prolonged anesthesia.

Fig. 4a shows an exemplary response family recorded at 39.0°C body temperature and Fig. 4b shows an exemplary body temperature alteration over time. Responses used in the final analysis were acquired when the body temperature was deemed stable, shown with black bars in the Fig. 4b. The effect of temperature on the dim and bright flash responses are shown in Fig. 4c and Fig. 4d, respectively. The time axis scaling transformation closely described the effects of temperature change on the a-

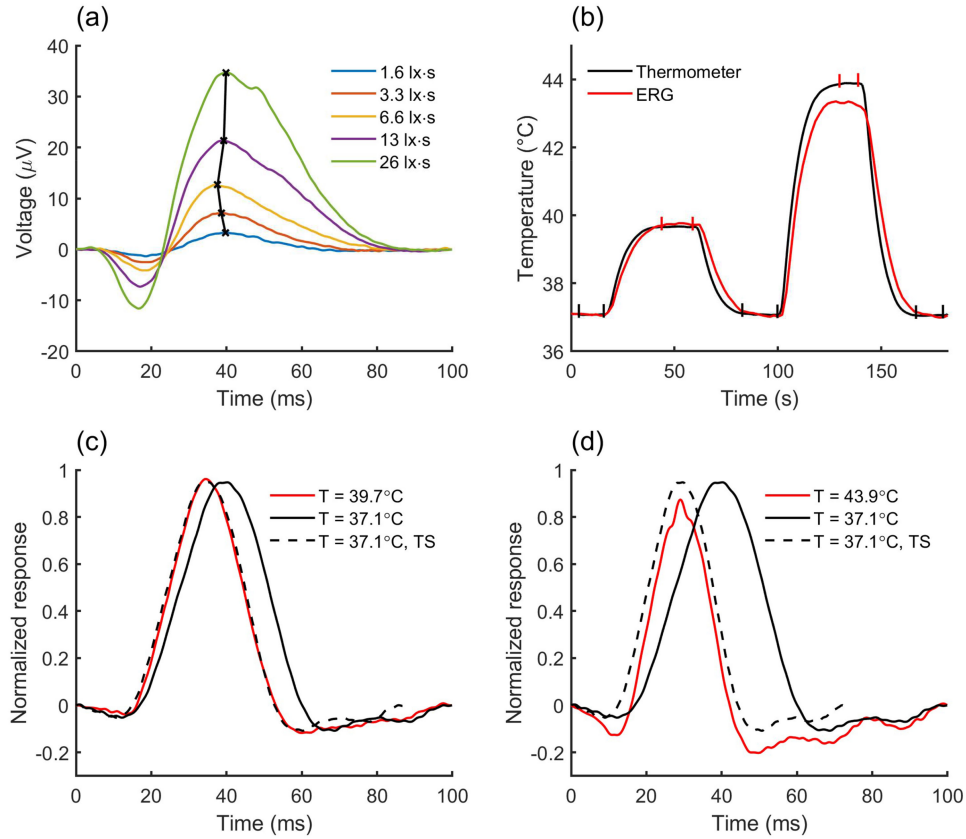

Fig. 2. (a) A response family acquired with 2x stimulus strength increments, with the flash strength delivered in a single flash shown in legend. The vertical dashed line intersects with the shortest b-wave time-to-maximum. (b) Perfusion temperature (black trace) and temperature determined from ERG (red trace) during two temperature alterations with the flash strength producing the shortest b-wave time-to-maximum. Responses acquired at stable reference and altered temperatures (time intervals marked with black and red markers, respectively) were averaged and used in further analysis. (c) & (d) Examples of ERG responses recorded at a reference temperature (black solid line) and an altered temperature (red solid line) acquired with a luminous exposure of 676 lx·s per stimulus. The dashed black trace shows the response recorded at the reference temperature with a time axis scaling (TS) that maximizes the correlation with the response recorded at an altered temperature. A 21 lx background illumination was used in all ex vivo recordings to ensure suppression of rod responses.

and b-waves in the investigated temperature range with all used stimulus strengths.

Fig. 5a shows the average b-wave time-to-maximum (TTM) and normalized amplitude from all response families. The amplitudes shown in the figure are normalized by the b-wave amplitude produced by the strongest flash stimulus. The average peak-to-peak amplitude of the ERG response elicited with the brightest stimulus was 300 ± 130 μV (mean $\pm$ std). The average temperature of all response families was 38.0°C, and the standard deviation of the average of the two temperatures of each temperature alteration was 0.15°C. A flash illuminance of approximately 6 cd·s·m^{-2} produced the fastest cone driven b-wave, marking a comparable location in the dynamic range to the *ex vivo* data. Fig. 5b shows the temperature dependence of the time axis scaling feature with different flash strengths. Results from responses elicited with $<$1.7 cd·s·m^{-2} were omitted due to low SNR. The temperature dependence was found to depend on flash strength, peaking at 4.7%/°C near 4 cd·s·m^{-2}, slightly below the strength corresponding to the ERG response with the fastest cone driven b-wave. This is close to the value discovered in *ex vivo* experiments at a comparable stimulus strength (5.0%/°C). With brighter flashes the temperature dependence stabilized near the minimum value of 3.6%/°C within the investigated dynamic range.

C. Temperature Determination From ERG Signals With Low Signal-to-Noise Ratio

Ex vivo ERG recordings from isolated retinas and full-field ERG recordings from anaesthetized pigs have a high signal-to-noise ratio (SNR). However, in local laser treatment, the ERG stimulation should be limited within the treated area, resulting in small amplitudes for the recorded signals. With a lower signal-to-noise ratio (SNR), a higher number of ERG responses needs be acquired to generate a sufficiently clean response for temperature determination, requiring longer recording times. Hence, the signal noise becomes a significant determinant of temperature precision, setting a limit for the stimulation area and temporal resolution in ERG-based temperature determination.

The feasibility of ERG-based temperature determination from low amplitude signals was analyzed through simulations. The simulations tested the effect of ERG-signal amplitude and the

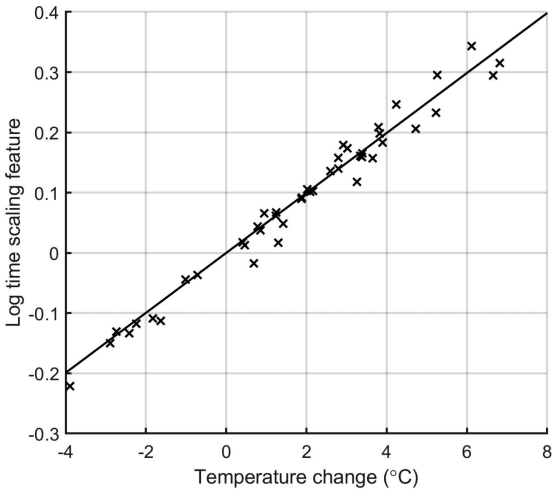

Fig. 3. Effect of temperature change on signaling kinetics of ex vivo ERG responses. The crosses describe the results of 44 individual temperature alterations from 8 retinal stamps while the black line shows the origin-intersecting linear fit on the data. The slope of the fit, 5.0%/°C, represents the temperature dependence of ex vivo ERG response kinetics.

number of averaged responses on the accuracy of the temperature estimates from ERG signals with a low SNR. Pure signal noise recorded with ERG electrodes was superimposed on series of full-field responses with downscaled amplitudes to mimic noisy focal ERG signals (see Methods for the simulation protocol). The noise used in the simulations was acquired in five separate recordings from different pigs. The full-field *in vivo* ERG responses used in the analysis of temperature dependence of ERG signaling kinetics were used as template responses in the simulation. The full-field ERG response amplitudes were scaled to 1, 2, 4 or 8 μV and series of 8 to 1024 responses were created from multiplicated responses.

Fig. 6 shows the error in the optimal time axis scaling feature (left axis) and the temperature error (right axis) with different signal amplitudes and numbers of averaged signals. The presented temperature error presumes a temperature dependence of 3.6%/°C, which is the temperature dependence observed with stronger stimuli. When the simulated SNR was extremely low, the optimal time scaling feature algorithm failed to find a correlation peak within the investigated time axis scaling interval. Iterations where the algorithm failed to determine the optimal time scaling feature were not used in the calculation of RMS error values. The results shown in Fig. 6 show the results for simulation parameters resulting in failure rates $<$ 5%. The simulation results are shown with solid lines, while the dashed lines show the curves from Eq. 6 fitted on the data, with $c = 0.45\mu V$ for optimal time scaling feature error or $c = 12°\mathrm{C}\mu V$ for temperature error, respectively.

The pig retina contains nearly 20 million cones, the average cone density being around 30 000 mm^{-2} at the visual streak [33]. As the amplitude of a fERG signal is proportional to the number of cone cells in the stimulated area, a 1 μV signal amplitude requires signaling from approximately 0.3% of the retinal cones assuming maximal full-field ERG amplitude of 300 μV. This translates to a circular spot diameter of approximately 1.7 mm, presuming that the stimulated area has the average cone density of 30 000 mm^{-2}. With the same premises, 3 mm diameter circular stimulation spot would produce signal amplitudes of approximately 3.2 μV. Plugging $c = 12°\mathrm{C}\mu V$ into Eq. 6 and using a stimulation frequency of 8 Hz, we may estimate that 14 seconds of signal recording is required for both of the compared responses (recorded at the reference and elevated temperature, respectively) to reach a noise related RMS temperature error of 0.5°C.

IV. Discussion

Subthreshold retinal laser therapy (SLT) is a promising treatment method for various retinal disorders [7]–[21]. However, current treatment devices lack temperature control, preventing the delivery of an optimal thermal dose. Here we show that the temperature-dependent ERG signal kinetics presents a potential probe for determining the temperature elevation caused by laser exposure, enabling safer and more effective treatments. This study examines the temperature dependence of ERG signaling kinetics in a broad temperature range with isolated isolated pig retinas, and the effect of different stimulus strengths with anesthetized pigs. The feasibility of using low SNR fERG responses to control the laser treatment is analyzed with computational simulations.

A single feature was extracted from pairs of ERG responses to quantify the changes in the signaling kinetics. The feature was designed to be robust with noisy ERG signals. It relies on finding how much the time axis of the ERG signal registered in an altered temperature needs to be scaled in order to maximize the similarity to an ERG signal registered in control conditions. Unlike time-to-peak values, which are extensively used to quantify ERG signaling kinetics, the optimal time scaling feature samples the compared signals broadly, making it more resilient with low SNR signals. The optimal time scaling feature changed with a constant slope of 5.0%/°C when the temperature of the retinal stamp was altered in the range of 33 to 44°C while continuously collecting photopic ERG responses. The responses recorded from anesthetized pigs at different temperatures revealed that the temperature dependence of photopic ERG signaling kinetics depends on the flash strength. The temperature dependence varied between 3.6 and 4.7%/°C, peaking at low flash strength and stabilizing towards high flash strengths (see Fig. 5b).

To utilize the ERG-based temperature determination during laser treatment, the ERG responses should be collected inside the heated area. This can be achieved with focal ERG (fERG) technique where only a small portion of the retina is stimulated to induce a local response [27]. The temperature dependence of the mouse rod-mediated ERG has been earlier investigated both *ex vivo* and *in vivo* [25], [26]. However, cone-driven fERG has clear advantages over rod-driven fERG during laser treatment regarding the simplicity of the stimulation protocols, the suppression of stray light artefacts, and the signal-to-noise ratio due to faster signaling kinetics of cones and their ability to remain responsive in bright background light. Our study shows that the change in

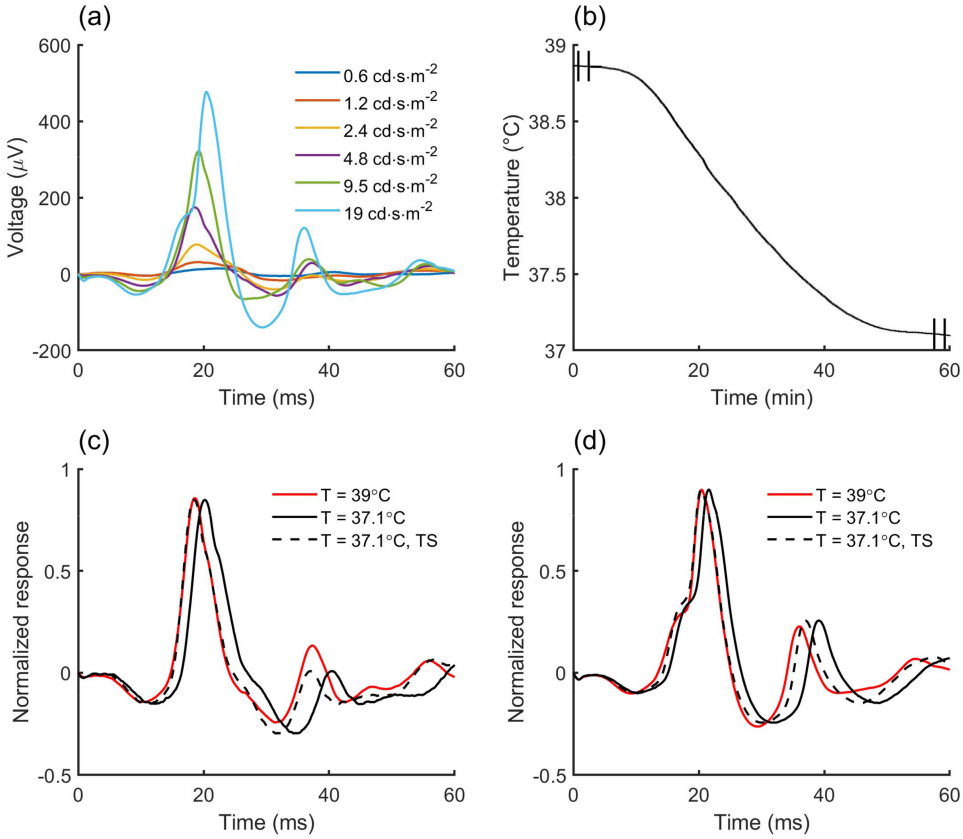

Fig. 4. (a) In vivo photopic flash response family with 2-fold increment in flash strength (part of the acquired responses were omitted for clarity). (b) Exemplary temperature alteration with stable time intervals for ERG recordings shown with black lines. (c) & (d) Photopic flash responses recorded with 5.6 cd·s·m^{-2} and 19 cd·s·m^{-2} flash strengths, respectively, at temperatures 37.1°C (black solid line) and 39°C (red solid line) at a background of 300 cd·m^{-2}. The dashed black line shows the response recorded at 37.1°C with the time axis scaled so that it maximizes the correlation with the response recorded at 39°C.

the cone-mediated photopic ERG signal kinetics of the pig retina has a strong temperature dependence similarly as shown before for mouse rod-mediated ERG [25], [26]. The result suggests that the presented method provides a potential temperature probe when be used with cone-driven fERG signals acquired inside the area of laser exposure during an SLT protocol. With a long laser pulse, retinal temperature stabilizes in approximately 15 seconds [34]. To determine the steady-state retinal temperature elevation, ERG responses acquired before laser exposure could be compared to responses acquired after the first 15 seconds of laser exposure.

The laser exposure itself has certain constraints to enable ERG based retinal temperature determination, namely the requirement that the laser wavelength should be in the near-infrared region to prevent excessive light adaptation from the laser exposure, and that the laser spot should be sufficiently large and the exposure sufficiently long to acquire fERG signals of acceptable SNR for temperature determination. In this study, we used computational simulations to assess the feasibility of ERG-based retinal temperature determination from noisy fERG signals. The temporal resolution of the method depends on various factors, i.e., the used electrode and fundus lens combination, the amplitude of the induced ERG signal from the targeted retinal area, and the signal artefacts produced by the subject. The simulations provided a rough estimate of the temperature-determination error with different ERG signal amplitudes and recording times when using a conventional DTL electrode and contact fundus lens. According to our simulations, a laser spot diameter of > 3 mm would allow temperature determination from the heated area with 15 seconds of ERG acquisition. As it takes approximately 15 seconds for retinal temperature to stabilize, the method can approximate the steady state temperature elevation of a 30 second laser exposure. However, optimizing the stimulation and signal processing protocols, as well as the electrode system could improve the robustness and temporal resolution of the method.

The a-b-wave complex of ERG signal originates in the photoreceptor and bipolar layers of the retina [35]. The signal arises in the photoreceptor outer segments that are partially embedded in the RPE, which is the strongest absorber of the light energy during laser treatments [36]. Hence, the temperature of the photoreceptor outer segments should closely correspond to the temperature of the RPE. Noteworthy is that during multisecond laser exposure, the temperature of the whole, around 300 μm thick retina should correspond to or be only slightly lower than the temperature of the RPE [37], [38]. Yet, to conclusively

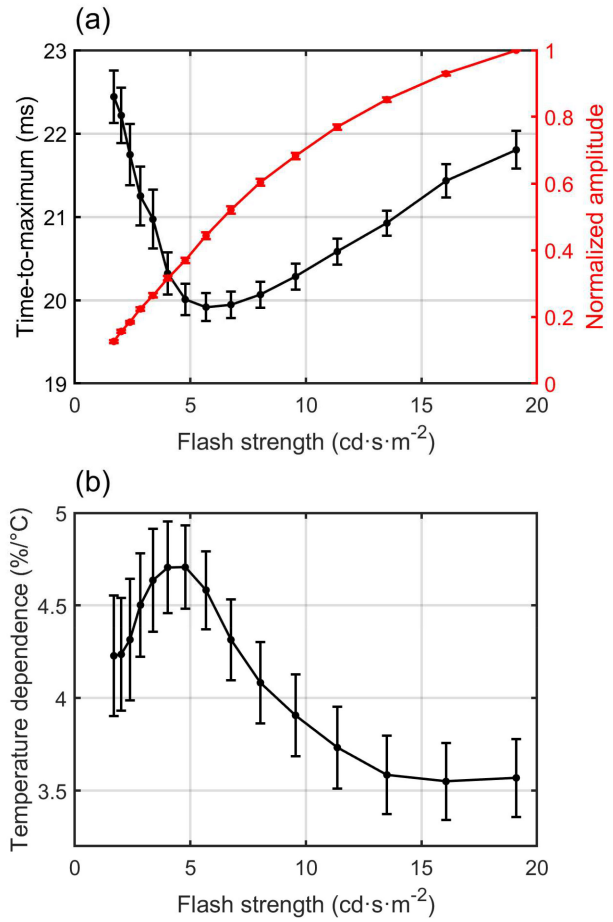

Fig. 5. (a) The average b-wave time-to-maximum (TTM, left vertical axis), and normalized peak-to-peak amplitude of the a-b-wave complex (right vertical axis) with different flash strengths. The error bars indicate the standard error of mean (SEM) of the average TTM and normalized amplitude of the response families recorded before and after each temperature alteration. The amplitude with the brightest flash was scaled to 1. (b) The average temperature dependence of kinetics acceleration with different flash strengths in 300 cd·m^{-2} background light. The error bars indicate SEMs from all of the temperature alterations.

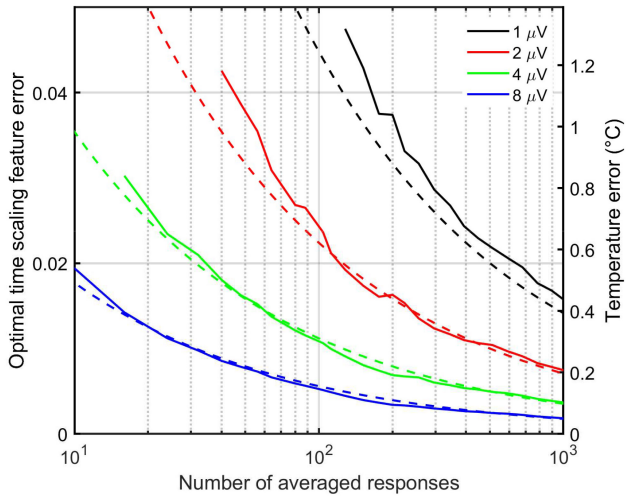

Fig. 6. RMS error of the optimal time axis scaling feature (left axis) and the corresponding temperature error (right axis) caused by signal noise with different signal amplitudes (solid traces for simulation data, dashed lines for fits according to Eq. 6) and numbers of averaged responses (horizontal axis, log-scale).

validate the accuracy of the method, a study examining the ability of the ERG-based retinal temperature method to predict laser treatment outcomes is warranted.

The most commonly used SLT methods deliver short bursts of microsecond-scale pulses to cover the treatment area with small non-damaging treatment spots [10]. The method allows the tissue to cool between pulses and restricts the temperature increase close to the RPE layer [39], which minimizes the collateral damage in case of overtreatment. Another method, transpupillary thermotherapy (TTT), aims to heat RPE, retina and choroid by around 10°C using a 60-second laser pulse covering the whole treated area [40]. Potency of TTT in treating central serous chorioretinopathy [14]–[18], [41]–[43] and possibly lessening the need for anti-VEGF injections for wet AMD [21] have been shown in clinical trials. However, largely due to suboptimal thermal dosing and safety concerns arising from treating a large area without temperature control, subthreshold TTT never reached widespread clinical use.

The laser-induced therapeutic effect and the retinal damage seems to be defined by the delivered thermal dose rather than chosen treatment modality and parameters [39], [44], [45]. Although the main hypothesis is that the treatment effect is induced by the heating of the RPE [3], [23], [24], [40], it is unclear whether limiting the therapeutic effect to the RPE is necessary or even beneficial if safety concerns associated with SLT could be alleviated. The introduced ERG-based temperature control would enable the optimal thermal dose to be delivered reliably without significant risks for adverse events for long pulse laser treatments such as TTT [21], [40]. This would enable safe comparison of treatment modalities and choosing the most potent method for different retinal diseases.

V. Conclusion

In this study, we quantified the temperature dependence of cone-driven ERG flash responses in the domestic pig retina, both *ex vivo* from isolated retinas and *in vivo* from anaesthetized pigs. The temperature dependence of photopic ERG signaling kinetics peaked at 4.7%/°C with a relatively dim stimuli, and decreased to 3.6%/°C when the stimulus strength was increased. The temperature dependence was constant within the investigated range of 33 to 44°C. The high temperature dependence makes ERG a potential probe to estimate the temperature elevation during SLT, where a portion of the RPE is heated to non-damaging temperatures. However, ERG signals should be collected within the limited retinal area heated during SLT, leading to low amplitudes. The feasibility of ERG-based temperature control for SLT using low amplitude fERG signals was assessed through computational simulations. The simulations showed that the method can be used to determine retinal temperature from a

3 mm diameter retinal spot in < 15 seconds with high precision. This makes the method suitable for controlling laser treatments such as transpupillary thermotherapy where the laser exposure duration is typically 60 seconds. Noteworthy is that the simulations take into account only the signal-to-noise ratio of the ERG signals and other confounding factors might arise during clinical use. Hence, an additional study where the ERG-based temperature determination is used during laser treatment would further validate the feasibility of the method. Accurate thermal dosimetry could improve the repeatability, safety, and efficacy of SLT, which has already shown its potential for treating various retinal diseases.

Acknowledgment

Authors O.K. and T.T have equity interest in Maculaser Ltd, whose business is related to the content of this paper and which was founded after acquiring and analyzing the data presented in this paper.

References

[1] K. Inagaki *et al.*, "Sublethal photothermal stimulation with a micropulse laser induces heat shock protein expression in ARPE-19 cells," *J. Ophthalmol.*, vol. 2015, 2015, Art. no. 729792, doi: 10.1155/2015/729792.

[2] Y. Morimura *et al.*, "Histological effect and protein expression in subthreshold transpupillary thermotherapy in rabbit eyes," *Arch. Ophthalmol.*, vol. 122, no. 10, pp. 1510–1515, 2004, doi: 10.1001/archopht.122.10.1510.

[3] K. Kern *et al.*, "Expression of heat shock protein 70 and cell death kinetics after different thermal impacts on cultured retinal pigment epithelial cells," *Exp. Eye Res.*, vol. 170, pp. 117–126, 2018, doi: 10.1016/j.exer.2018.02.013.

[4] S. De Cillà *et al.*, "The subthreshold micropulse laser treatment of the retina restores the oxidant/antioxidant balance and counteracts programmed forms of cell death in the mice eyes," *Acta Ophthalmol.*, vol. 97, no. 4, pp. e559–e567, Dec. 2019, doi: 10.1111/aos.13995.

[5] J. Tode *et al.*, "Thermal stimulation of the retina reduces bruch's membrane thickness in age related macular degeneration mouse models," *Transl. Vis. Sci. Technol.*, vol. 7, no. 3, 2018, Art. no. 2, doi: 10.1167/tvst.7.3.2.

[6] Z. Li *et al.*, "Biological modulation of mouse RPE cells in response to subthreshold diode micropulse laser treatment," *Cell Biochem. Biophys.*, vol. 73, no. 2, pp. 545–552, Nov. 2015, doi: 10.1007/s12013-015-0675-8.

[7] Y. Wu *et al.*, "Subthreshold diode micropulse laser versus conventional laser photocoagulation monotherapy or combined with anti-VEGF therapy for diabetic macular edema: A Bayesian network meta-analysis," *Biomed. Pharmacother.*, vol. 97. pp. 293–299, Jan. 2018, doi: 10.1016/j.biopha.2017.10.078.

[8] G. Chen *et al.*, "Subthreshold micropulse diode laser versus conventional laser photocoagulation for diabetic macular edema," *Retina*, vol. 36, no. 11, pp. 2059–2065, Nov. 2016, doi: 10.1097/IAE.0000000000001053.

[9] P. Scholz, L. Altay, and S. Fauser, "A review of subthreshold micropulse laser for treatment of macular disorders," *Adv. Ther.*, vol. 34, no. 7. pp. 1528–1555, Jul. 2017, doi: 10.1007/s12325-017-0559-y.

[10] M. Gawęcki, "Micropulse laser treatment of retinal diseases," *J. Clin. Med.*, vol. 8, no. 2, Feb. 2019, Art. no. 242, doi: 10.3390/jcm8020242.

[11] J. K. Luttrull, D. C. Musch, and C. A. Spink, "Subthreshold diode micropulse panretinal photocoagulation for proliferative diabetic retinopathy," *Eye*, vol. 22, no. 5, pp. 607–612, May 2008, doi: 10.1038/sj.eye.6702725.

[12] M. Jhingan *et al.*, "Subthreshold microsecond laser for proliferative diabetic retinopathy: A randomized pilot study," *Clin. Ophthalmol.*, vol. 12, pp. 141–145, 2018, doi: 10.2147/OPTH.S143206.

[13] Z. Sun *et al.*, "Efficacy and safety of subthreshold micropulse laser compared with threshold conventional laser in central serous chorioretinopathy," *Eye*, vol. 34, no. 9, pp. 1592–1599, Nov. 2020, doi: 10.1038/s41433-019-0692-8.

[14] D. Shukla *et al.*, "Transpupillary thermotherapy for subfoveal leaks in central serous chorioretinopathy," *Eye*, vol. 22, no. 1, pp. 100–106, Jan. 2008, doi: 10.1038/sj.eye.6702449.

[15] G. J. Manayath *et al.*, "Low fluence photodynamic therapy versus graded subthreshold transpupillary thermotherapy for chronic central serous chorioretinopathy: Results from a prospective study," *Ophthalmic Surg. Lasers Imag. Retin.*, vol. 48, no. 4, pp. 334–338, Apr. 2017, doi: 10.3928/23258160-20170329-08.

[16] G. lo Giudice *et al.*, "Large-spot subthreshold transpupillary thermotherapy for chronic serous macular detachment," *Clin. Ophthalmol.*, vol. 5, no. 1, pp. 355–360, Mar. 2011, doi: 10.2147/OPTH.S16014.

[17] V. Mathur *et al.*, "Role of transpupillary thermotherapy in central serous chorio-retinopathy," *Med. J. Armed Forces India*, vol. 65, no. 4, pp. 323–327, Oct. 2009, doi: 10.1016/S0377-1237(09)80092-0.

[18] N. Hussain *et al.*, "Transpupillary thermotherapy for chronic central serous chorioretinopathy," *Graefe's Arch. Clin. Exp. Ophthalmol.*, vol. 244, no. 8, pp. 1045–1051, Aug. 2006, doi: 10.1007/s00417-005-0175-4.

[19] J. K. Luttrull *et al.*, "Low incidence of choroidal neovascularization following subthreshold diode micropulse laser (SDM) in high-risk AMD," *PLoS One*, vol. 13, no. 8, 2018, Art. no. e0202097, doi: 10.1371/journal.pone.0202097.

[20] J. K. Luttrull *et al.*, "Slowed progression of age-related geographic atrophy following subthreshold laser," *Clin. Ophthalmol.*, vol. 14, pp. 2983–2993, 2020, doi: 10.2147/OPTH.S268322.

[21] A. C. Söderberg *et al.*, "Combination therapy with low-dose transpupillary thermotherapy and intravitreal ranibizumab for neovascular age-related macular degeneration: A 24-month prospective randomised clinical study," *Br. J. Ophthalmol.*, vol. 96, no. 5, pp. 714–718, Apr. 2012, doi: 10.1136/bjophthalmol-2011-300721.

[22] T. Desmettre, C. A. Maurage, and S. Mordon, "Heat shock protein hyperexpression on chorioretinal layers after transpupillary thermotherapy," *Investig. Ophthalmol. Vis. Sci.*, vol. 42, no. 12, pp. 2976–2980, Nov. 2001.

[23] C. Sramek *et al.*, "Non-damaging retinal phototherapy: Dynamic range of heat shock protein expression," *Investig. Ophthalmol. Vis. Sci.*, vol. 52, no. 3, pp. 1780–1787, Mar. 2011, doi: 10.1167/iovs.10-5917.

[24] M. Amirkavei *et al.*, "Induction of heat shock protein 70 in mouse RPE as an in vivo model of transpupillary thermal stimulation," *Int. J. Mol. Sci.*, vol. 21, no. 6, Mar. 2020, Art. no. 2063, doi: 10.3390/ijms21062063.

[25] M. Pitkänen, O. Kaikkonen, and A. Koskelainen, "A novel method for mouse retinal temperature determination based on ERG photoresponses," *Ann. Biomed. Eng.*, vol. 45, no. 10, pp. 2360–2372, 2017, doi: 10.1007/s10439-017-1872-y.

[26] M. Pitkänen, O. Kaikkonen, and A. Koskelainen, "In vivo monitoring of mouse retinal temperature by ERG photoresponses," *Exp. Eye Res.*, vol. 187, May 2019, Art. no. 107675, doi: 10.1016/j.exer.2019.05.015.

[27] M. Sandberg, B. Pawlyk, and E. Berson, "Isolation of focal rod electroretinograms from the dark-adapted human eye," *Invest. Ophthalmol. Vis. Sci.*, vol. 37, pp. 930–934, May 1996.

[28] A. Binns and T. H. Margrain, "Development of a technique for recording the focal rod ERG," *Ophthalmic Physiol. Opt.*, vol. 26, no. 1, pp. 71–79, Feb. 2006, doi: 10.1111/j.1475-1313.2005.00355.x.

[29] S. Machida *et al.*, "Comparison of photopic negative response of full-field and focal electroretinograms in detecting glaucomatous eyes," *J. Ophthalmol.*, vol. 2011, pp. 1–11, vol. 2011, doi: 10.1155/2011/564131.

[30] S. Machida, "Clinical applications of the photopic negative response to optic nerve and retinal diseases," *J. Ophthalmol.*, vol. 2012, p. 11, 2012, Art. no. 397178, doi: 10.1155/2012/397178.

[31] K. Tamada *et al.*, "Photopic negative response of full-field and focal macular electroretinograms in patients with optic nerve atrophy," *Jpn. J. Ophthalmol.*, vol. 53, no. 6, pp. 608–614, 2009, doi: 10.1007/s10384-009-0731-2.

[32] M. Kondo *et al.*, "Comparison of focal macular cone ERGs in complete-type congenital stationary night blindness and APB-treated monkeys," *Vis. Res,* vol. 48, no. 2, pp. 273–280, 2008, doi: 10.1016/j.visres.2007.11.010.

[33] A. Hendrickson and D. Hicks, "Distribution and density of medium- and short-wavelength selective cones in the domestic pig retina," *Exp. Eye Res.*, vol. 74, pp. 435–444, May 2002, doi: 10.1006/exer.2002.1181.

[34] J. Kandulla *et al.*, "Noninvasive optoacoustic online retinal temperature determination during continuous-wave laser irradiation," *J. Biomed. Opt.*, vol. 11, no. 4, 2006, Art. no. 041111, doi: 10.1117/1.2236301.

[35] E. N. Pugh, B. Falsini, and A. L. Lyubarsky, "The origin of the major rod- and cone-driven components of the rodent electroretinogram and the effect of age and light-rearing history on the magnitude of these components," in *Photostasis and Related Phenomena*, T. P. Williams and A. B. Thistle, Eds. Boston, MA, USA: Springer, 1998, pp. 93–128, doi: 10.1007/978-1-4899-1549-8_7.

[36] S. C. Finnemann and Y. Chang, "Photoreceptor—RPE interactions," in *Visual Transduction and Non-Visual Light Perception*, J. Tombran-Tink and C. J. Barnstable, Eds. Totowa, NJ, USA: Humana Press, 2008, pp. 67–86.

[37] M. A. Mainster *et al.*, "Retinal-temperature increases produced by intense light sources," *J. Opt. Soc. Amer.*, vol. 60, no. 2, pp. 264–270, Feb. 1970, doi: 10.1364/josa.60.000264.

[38] S. Grover *et al.*, "Comparison of retinal thickness in normal eyes using stratus and spectralis optical coherence tomography," *Investig. Ophthalmol. Vis. Sci.*, vol. 51, no. 5, pp. 2644–2647, 2010, doi: 10.1167/iovs.09-4774.

[39] J. Wang *et al.*, "Comparison of continuous-wave and micropulse modulation in retinal laser therapy," *Investig. Ophthalmol. Vis. Sci.*, vol. 58, no. 11, pp. 4722–4732, Sep. 2017, doi: 10.1167/iovs.17-21610.

[40] M. A. Mainster and E. Reichel, "Transpupillary thermotherapy for age-related macular degeneration long-pulse photocoagulation, apoptosis, and heat shock proteins," *Ophthalmic Surg. Lasers*, vol. 31, no. 5, pp. 359–373, 2000.

[41] G. J. Manayath *et al.*, "Graded subthreshold transpupillary thermotherapy for chronic central serous chorioretinopathy," *Ophthalmic Surg. Lasers Imag.*, vol. 43, no. 4, pp. 284–290, Jul. 2012, doi: 10.3928/15428877-20120618-06.

[42] R. Kawamura *et al.*, "Transpupillary thermotherapy for atypical central serous chorioretinopathy," *Clin. Ophthalmol.*, vol. 6, no. 1, pp. 175–179, 2012, doi: 10.2147/OPTH.S28239.

[43] A. Russo *et al.*, "Comparison of half-dose photodynamic therapy and 689 nm laser treatment in eyes with chronic central serous chorioretinopathy," *Graefe's Arch. Clin. Exp. Ophthalmol.*, vol. 255, no. 6, pp. 1141–1148, Jun. 2017, doi: 10.1007/s00417-017-3626-9.

[44] J. Chhablani *et al.*, "Comparison of different settings for yellow subthreshold laser treatment in diabetic macular edema," *BMC Ophthalmol.*, vol. 18, no. 1, Jul. 2018, Art. no. 168, doi: 10.1186/s12886-018-0841-z.

[45] S. Vujosevic *et al.*, "Subthreshold micropulse yellow laser versus subthreshold micropulse infrared laser in center-involving diabetic macular edema," *Retina*, vol. 35, no. 8, pp. 1594–1603, Aug. 2015, doi: 10.1097/IAE.0000000000000521.